ADVANCED OPTICAL MATERIALS
www.advopticalmat.de

Catalyst-Free Vapor–Solid Deposition Growth of β-Ga_2O_3 Nanowires for DUV Photodetector and Image Sensor Application

*Chao Xie, Xing-Tong Lu, Meng-Ru Ma, Xiao-Wei Tong, Zhi-Xiang Zhang, Li Wang, Chun-Yan Wu, Wen-Hua Yang, and Lin-Bao Luo**

Photodetection in the solar-blind deep-ultraviolet (DUV) regime (200–280 nm) has received significant attention for its many critical applications in military and civil areas. In this study, a vapor–solid synthesis technique for catalyst-free growth of single-crystalline β-Ga_2O_3 nanowires is developed. A photodetector made of the nanowires is highly sensitive to 265 nm DUV illumination with excellent photoresponse performance. The performance parameters including I_{light}/I_{dark} ratio, responsivity, specific detectivity and response speed can attain ≈10^3, ≈233 A W^{-1}, ≈8.16×10^{12} Jones, and 0.48/0.04 s, respectively. Additionally, the detector has an abrupt response cutoff wavelength at ≈290 nm with a reasonable DUV/visible (250–405 nm) rejection ratio exceeding 10^2. It is also found that the device can operate properly at a large applied bias of 200 V with the responsivity being enhanced to as high as ≈1680 A W^{-1}. Moreover, such a nanowires-based photodetector can function as a DUV light image sensor with a reasonable spatial resolution. Holding the above advantages, the present DUV photodetector based on catalyst-free grown β-Ga_2O_3 nanowires possesses huge possibility for application in future DUV optoelectronics.

1. Introduction

Solar radiation in the waveband of 200–280 nm cannot reach the surface of the Earth due to absorption of ozone and atmosphere layers, for which the waveband of 200–280 nm is typically defined as solar-blind deep-ultraviolet (DUV) spectrum region.[1,2] Light detection in this region has lately received enormous and ever growing attention because of its vast applications for many civil and military purposes including missile warning, flame detection, remote control, chemical and biological analysis, and secure space-to-space communications.[3,4] In the past decade, a variety of ultrawide-bandgap (UWBG) semiconductors (e.g., $Zn_xMg_{1-x}O$, $Al_xGa_{1-x}N$, diamond, and gallium oxide (Ga_2O_3)) have been explored for constructing DUV photodetectors.[2–5] This class of semiconductors typically has bandgaps significantly larger than the 3.4 eV of GaN,[6] rendering them especially suitable for solar-blind DUV photodetection. Extensive studies have proven that UWBG semiconductor photodetectors can exhibit apparent advantages over traditional DUV photodetectors (e.g., photomultiplier tubes and thermal detectors), which usually have drawbacks such as being bulky and heavy, high power consumption, slow, and wavelength-independent photoresponse. Among the UWBG semiconductors, the alloys of $Zn_xMg_{1-x}O$ and $Al_xGa_{1-x}N$ can realize solar-blind light detection only at high Mg and Al compositions, respectively, which are inevitably accompanied with the appearance of phase segregation in $Zn_xMg_{1-x}O$ alloy and deterioration of crystal quality in $Al_xGa_{1-x}N$ film.[7–10] The quantum efficiency of diamond-based detectors is usually low, and their spectral response is also limited to only below 225 nm, due to the large indirect bandgap (≈5.5 eV) of diamond.[5,11] On the other hand, monoclinic Ga_2O_3 (β-Ga_2O_3), as the most stable phase of Ga_2O_3, has a direct wide bandgap of 4.4–5.3 eV and can be synthesized in high quality. By this token, β-Ga_2O_3 has proven to be excellent building block for solar-blind DUV light detection.[12–14]

To date, a number of DUV photodetectors based on β-Ga_2O_3 in the form of either thin films or nanostructures have been successfully developed.[15–23] Benefiting from quantum confinement effect and remarkable surface/size effect, β-Ga_2O_3 nanostructures, in particular 1D β-Ga_2O_3 nanowires (NWs) or nanobelts (NBs), can exhibit attractive merits of better optical absorption, improved charge carrier transportation, and increased surface states to interact with surroundings, over their thin films' counterpart.[3,24] Therefore, significant progresses have been made in the growth of high-quality β-Ga_2O_3 NWs/NBs for DUV photodetectors' application.[25–29] For example, Feng et al. reported the synthesis of β-Ga_2O_3 NWs on Au-coated Si substrate by directly evaporating Ga under

Dr. C. Xie, X.-T. Lu, M.-R. Ma, X.-W. Tong, Z.-X. Zhang, Dr. L. Wang, Prof. C.-Y. Wu, Dr. W.-H. Yang, Prof. L.-B. Luo
School of Electronic Science and Applied Physics and Anhui Provincial Key Laboratory of Advanced Functional Materials and Devices
Hefei University of Technology
Hefei, Anhui 230009, China
E-mail: luolb@hfut.edu.cn
Z.-X. Zhang
School of Physics and Engineering and Key Laboratory of Material Physics of Ministry of Education
Zhengzhou University
Zhengzhou, Henan 450052, China
The ORCID identification number(s) for the author(s) of this article can be found under https://doi.org/10.1002/adom.201901257.

DOI: 10.1002/adom.201901257

controlled conditions.[25] A photodetector based on individual NW showed obvious sensitivity to 254 nm DUV light. By selective growth of β-Ga_2O_3 NWs' layer on prepatterned Au thin layers via a chemical vapor deposition (CVD) process, Li et al. have successfully constructed a DUV photodetector based on bridged structure of β-Ga_2O_3 NWs.[26] Such a device achieved a responsivity of $\approx 10^{-2}$ A W^{-1} in the DUV region, with a high 250–280 nm rejection exceeding 10^3. In addition, by using metallic Ga and oxygen as precursor materials, β-Ga_2O_3 NBs can be prepared on Au colloids covering Si substrate as well.[27] A detector made of individual NB exhibited a responsivity of 39.2 A W^{-1} under 250 nm irradiation, which could be further improved by doping the NBs with In element.[30] Generally, these 1D β-Ga_2O_3 nanostructures are grown by a vapor–liquid–solid (VLS) mechanism, which is characterized by using noble metal nanoparticles (the most common catalyst is Au) as growth catalysts.[18,25–27,30] The use of metallic catalyst indeed can lead to high-quality material. Nonetheless, the residual Au acting as impurity in VLS-grown NWs/NBs is usually detrimental to the performance of NWs/NBs-based devices,[31,32] and Au is also incompatible with industrial electronic production standards.[33] Therefore, it is demanded to develop new techniques for catalyst-free growth of high-quality β-Ga_2O_3 NWs/NBs toward high-performance DUV light detection. Recently, Girija et al. reported the catalyst-free preparation of morphologically different β-Ga_2O_3 nanostructures.[34] However, the as-prepared products are nanorod-like structures with ultrashort lengths (shorter than 1 μm), which inevitably bring about difficulties in device fabrication and limits their applications. What is more, the optoelectronic properties of these nanostructures are also unknown.

Herein, we present the growth of single-crystalline β-Ga_2O_3 NWs via a vapor–solid (VS) mechanism without the use of any metallic catalysts or additives. Optoelectrical analysis reveals that photodetectors made of the as-synthesized NWs are highly sensitive to 265 nm DUV light irradiation, with excellent photoresponse performance in terms of a high I_{light}/I_{dark} ratio of $\approx 10^3$, a decent responsivity of ≈233 A W^{-1}, a large specific detectivity of $\approx 8.16 \times 10^{12}$ Jones, and a relatively fast response speed of 0.48/0.04 s. In addition, a sharp cutoff wavelength at around 290 nm and a reasonable DUV/visible (250–405 nm) rejection ratio exceeding 10^2 are observed. It is also found that the device can still work properly at a large applied bias of 200 V with a responsivity value as high as ≈1680 A W^{-1}, indicative of great potential for high-power optoelectronic applications. Furthermore, the present photodetector can reliably record a simple "smiley face" image produced by the DUV light with a decent spatial resolution. The above results suggest that the present device made of catalyst-free grown β-Ga_2O_3 NWs holds great potential for future DUV optoelectronic application.

2. Results and Discussion

In this work, the β-Ga_2O_3 NWs were synthesized via a catalyst-free VS mechanism in a tube furnace. The setup for growth of the β-Ga_2O_3 NWs is schematically shown in Figure S1a (Supporting Information), and the detailed procedures is provided in the "Experimental Section." To optimize the growth condition, control experiments were conducted by adjusting the growth temperature or flow rate of O_2 gas while keeping other parameters unchanged. **Figure 1**a–c depicts typical field-emission scanning electron microscopy (FESEM) images of the as-synthesized products at different growth temperatures of 700, 900, and 1100 °C, respectively. It was observed that at a growth temperature of 700 or 900 °C, the resultant products are composed of thick microrods or irregularly shaped microstructures with rough surfaces. While large-scale NWs with smooth surfaces and high aspect ratios can be obtained when raising the growth temperature to 1100 °C, the NWs have lengths of hundreds of micrometers and diameters of 100–500 nm. In addition, the flow rate of O_2 has a great influence on the morphology and density of the resultant NWs as well, as shown in Figure 1c,d. When reducing the O_2 flow rate from 50 to 20 SCCM (standard cubic centimeter per minute), only a tiny amount of NWs with length of several micrometers can be observed. In light of the above, the growth temperature and flow rate of O_2 are optimally chosen to be 1100 °C and 50 SCCM, respectively, in our experiments.

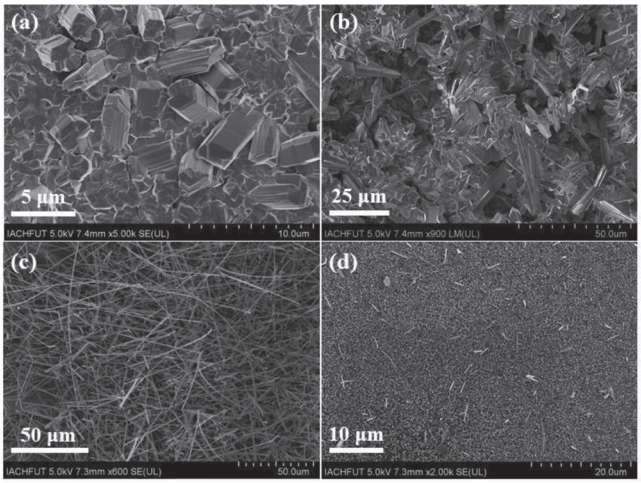

Figure 1. FESEM images of the β-Ga_2O_3 structures grown at different temperatures of a) 700, b) 900, and c) 1100 °C, respectively. The flow rate of O_2 gas is 50 SCCM. d) FESEM image of the β-Ga_2O_3 structures grown under the O_2 flow rate of 20 SCCM. The grown temperature is 1100 °C.

Figure 2a displays a transmission electron microscopy (TEM) image of a representative β-Ga_2O_3 NW with a diameter of ≈150 nm grown at 1100 °C. A high-resolution TEM (HRTEM) image recorded on the tip of the NW (Figure 2b) reveals lattice fringes with *d*-spacings of 0.202 and 0.209 nm, which correspond to the $[\bar{1}12]$ and $[\bar{6}01]$ lattice planes of β-Ga_2O_3 crystal, respectively. The NW has a preferential growth direction along the $[\bar{6}01]$ direction. In addition, the corresponding selected-area electron diffraction (SEAD) pattern (Figure 2c) confirms that the as-synthesized NWs are structurally uniform single crystals. By measuring angles of reflections and their corresponding spacing distances of the crystal planes, the reflections with a strong intensity can be assigned to the $[\bar{1}12]$, $[\bar{6}01]$, and [511] zone axes of β-Ga_2O_3 phase, respectively. Furthermore, from the X-ray energy-dispersive spectrometer (EDS) profile of the NWs (Figure 2d), the atomic ratio of Ga:O is estimated to be 39.2:60.8. This value agrees well with the result from the X-ray photoelectron spectroscopy (XPS) analysis (Figure S1b–d, Supporting Information) and is also very close to the stoichiometric

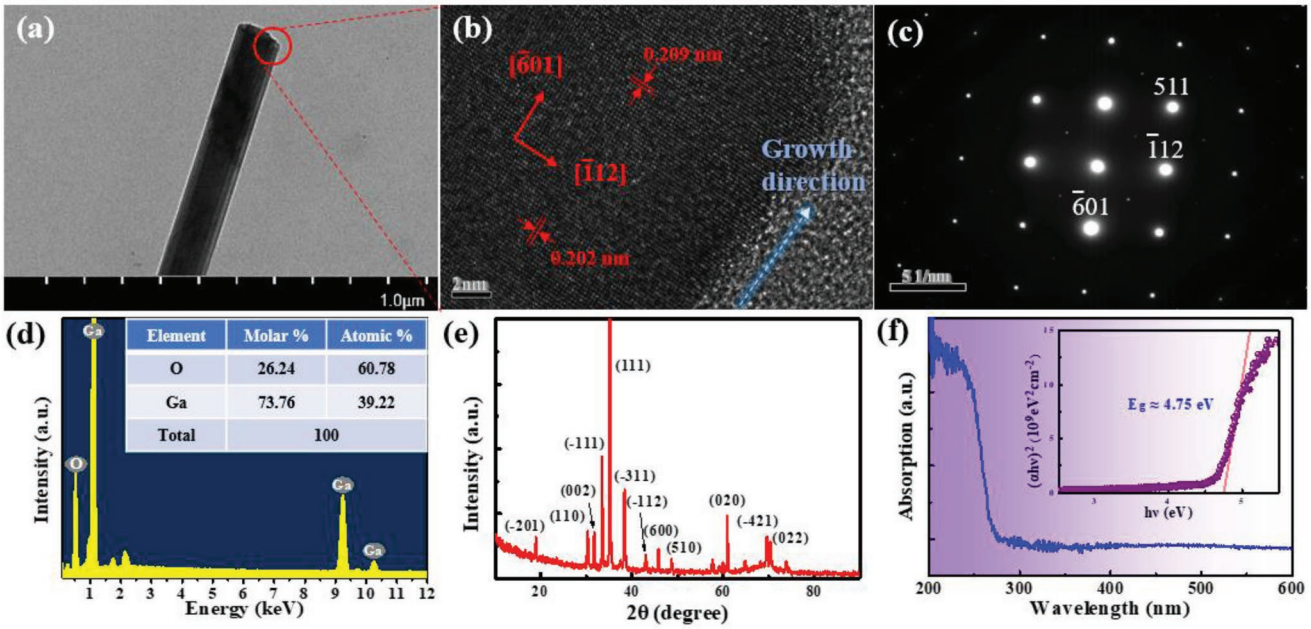

Figure 2. a) TEM image of a single β-Ga_2O_3 NW. b) HRTEM image recorded on the tip of the NW and c) the corresponding SEAD pattern. d) EDS spectrum, e) XRD pattern, and f) absorption spectrum of the β-Ga_2O_3 NWs. The inset in panel (f) shows the plot of $(\alpha h\nu)^2$ versus $h\nu$ for determining the optical bandgap of the β-Ga_2O_3 NWs.

ratio of Ga_2O_3. Figure 2e depicts the X-ray diffraction (XRD) pattern, in which all the diffraction peaks can be readily indexed to the monoclinic β-Ga_2O_3 with calculated lattice parameters a = 1.227 nm, b = 0.310 nm, c = 0.585 nm, and β = 103.3°, which are consistent with the standard values for bulk β-Ga_2O_3 (JCPDS Card No. 43–1012,).[25,26] Figure 2f plots the absorption spectrum of the β-Ga_2O_3 NWs, from which strong absorption at DUV wavelength region of 200–280 nm with a sharp absorption edge located at ≈290 nm is observed. In addition, by extrapolating the curve of $(\alpha h\nu)^2$–$h\nu$ (where α represents absorbance, h represents Planck's constant, and ν represents frequency) to zero intensity (inset in Figure 2f), the optical bandgap of the NWs is determined to be ≈4.75 eV, which coincides with the values in previous reports.[12,13] The above results confirm that β-Ga_2O_3 NWs with high-crystalline quality have been successfully synthesized.

By using β-Ga_2O_3 NWs as building blocks, a new DUV nano-photodetectors with a typical metal–semiconductor–metal (MSM) geometry was then fabricated. The inset in **Figure 3**a presents the optical image of the fabricated devices and the SEM image of a NWs-based DUV detector. The current–voltage (I–V) curve of a representative DUV detector was first measured in dark. As depicted in Figure S3a (Supporting Information), the device exhibited a low dark current of only ≈80 pA at a bias of 10 V with a nonlinear behavior, indicating the presence of Schottky barriers between NWs and electrode contacts, which is likely caused by the existence of many surface states on the β-Ga_2O_3 NWs.[12,35] Figure 3a compares the I–V curves in dark and under 265 and 365 nm illuminations with the same intensity (2.1 mW cm^{-2}), respectively. Apparently, the current increased drastically by ≈3 orders of magnitude when shinned by 265 nm irradiation, but kept nearly unchanged under 365 nm illumination, implying solar-blind photoresponsivity. Further study of the time-dependent photoresponse under periodically switched light illuminations in Figure 3b finds that the nano-photodetector can be readily turned between high- and low-current states upon 265 nm illumination with a good repeatability. The dark current was ≈10^{-10} A, while the current under light can reach as high as ≈2×10^{-7} A, giving a high I_{light}/I_{dark} ratio exceeding 2×10^3. As a matter of fact, such time-dependent photoresponse can keep nearly invariant even after hundreds of cycles of operation (Figure 3c), suggesting excellent operation reproducibility. In contrast, the device was almost insensitive to periodically switched 365 nm irradiation, which was consistent with the observation from the above I–V curves. In addition to the typically used Au electrodes, other metallic contact electrodes such as Ni or Pt were also employed in our experiments. The photoresponse properties of the devices with different contact electrodes and the same number of NWs across the channel were measured and compared, as shown in Figure S4 (Supporting Information). It was found that the photocurrent of devices with Ni or Pt electrodes was somewhat poorer than the detector with Au electrodes under the identical illumination condition. Besides the different work functions of varied metals, such an effect can probably be ascribed to the existence of surface states on the surface of β-Ga_2O_3 NWs as well, which may affect the contact between the NWs and metals.[3] Therefore, Au contact electrodes were chosen in this study. Furthermore, to shed light on the dependence of photoresponse on light wavelength, spectral photoresponse was recorded under illuminations with a constant intensity in the wavelength range of 200–600 nm (Figure 3d). It was observed that the device exhibited strong photoresponse for wavelengths from 200 to 280 nm, and the photoresponse began to decline abruptly at ≈290 nm. Under illuminations with wavelength longer

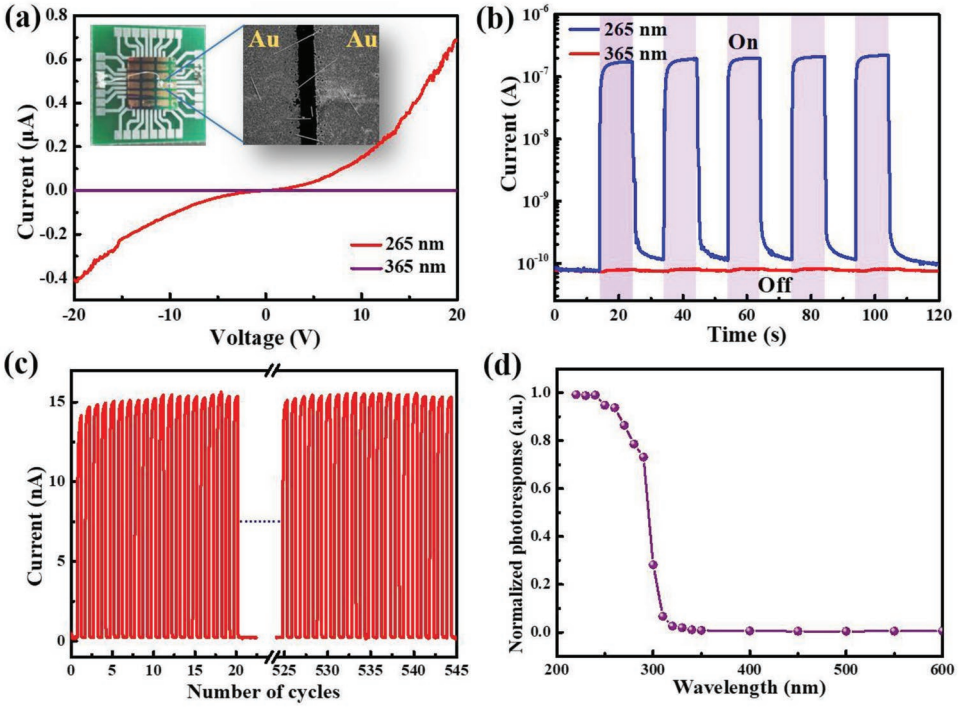

Figure 3. a) *I–V* curves of the β-Ga_2O_3 NWs-based photodetector measured in dark and under 265 and 365 nm illuminations. The inset shows the optical image of the devices and a typical SEM image of a NWs-based detector. Time-dependent photoresponse of the device b) under periodically switched 265 and 365 nm light illuminations (2.1 mW cm^{-2}) at a bias voltage of 10 V, and c) over hundreds of cycles of operation (265 nm, 450 μW cm^{-2}). d) Spectral photoresponse of the device in the wavelength range of 200–600 nm.

than 300 nm, the detector showed almost negligible photoresponse. The peak photoresponse was found to appear at the wavelength of ≈250 nm, implying that electron–hole pairs excited by DUV photons with energy higher than the bandgap of the NWs are responsible primarily for the photocurrent.[27] In addition, a large DUV/visible rejection ratio (250–405 nm) exceeding 10^2 was obtained. The above results suggest that the present β-Ga_2O_3 NWs-based detector can function as a solar-blind DUV photodetector with good spectral selectivity, high sensitivity, and robust reproducibility.

The photoresponse characteristics were found to depend strongly on the incident DUV light intensity. **Figure 4**a presents the *I–V* curves under 265 nm illumination with varied light intensities ranging from ≈0.68 to ≈994 μW cm^{-2}. Clearly, both currents at positive and negative bias voltages increased monotonously with increase in incident light intensity, which is understandable because light illumination with a higher intensity can excite more electron–hole pairs, which are contributory to photocurrent. To gain insight into such a dependence, we then fitted the curve of photocurrent at 10 V versus light intensity via a generally used power law: $I_{ph} \propto P^{\theta}$, where I_{ph} denotes the net photocurrent ($I_{ph} = I_{light} - I_{dark}$), P denotes the light intensity, and the exponent θ is an empirical value relating to the activities of photocarrier recombination.[36] Careful fitting the curve in the light intensity range of 0.68–994 μW cm^{-2} led to $\theta = 0.87$ (inset in Figure 4b), which deviates somewhat from the ideal value of 1 and implies the presence of photocurrent recombination loss at this light intensity region.[37] Furthermore, the time-dependent photoresponses were studied under 265 nm irradiation with different light intensities as well. As presented in Figure 4b, the photocurrent exhibited similar dependence on the light intensity. In addition, for all the illuminating conditions, the device can be readily switched between high- and low-current statuses, implying that the present DUV photodetector can work properly under light irradiations in a wide intensity range.

To quantitatively compare the performance of different DUV photodetectors, several critical performance parameters including responsivity (R) and external quantum efficiency (EQE) were then calculated. The R is defined as the photocurrent produced by unit power of incident light in the effective region of the photodetector, whereas EQE is described as the number of electrons detected by each incident photon. The two parameters are normally given by[38]

$$R = \frac{I_{ph}}{P_{\lambda} S} = \mathrm{EQE}\left(\frac{e\lambda}{hc}\right) \quad (1)$$

where P_{λ}, S, e, λ, h, and c represent the light intensity, the active illumination area ($S \cong 2.1 \times 10^{-6}$ cm^2), the elementary electronic charge (1.6×10^{-19} C), the wavelength of incident light, the Planck's constant, and the velocity of light, respectively. Based on the equation, the R and EQE values at the light intensity of 0.68 μW cm^{-2} were calculated to be ≈233 A W^{-1} and ≈1×10^5%, respectively. Both values are comparable to or even much higher than that of other β-Ga_2O_3 NWs- or NBs-based DUV photodetectors in previous reports working at similar bias

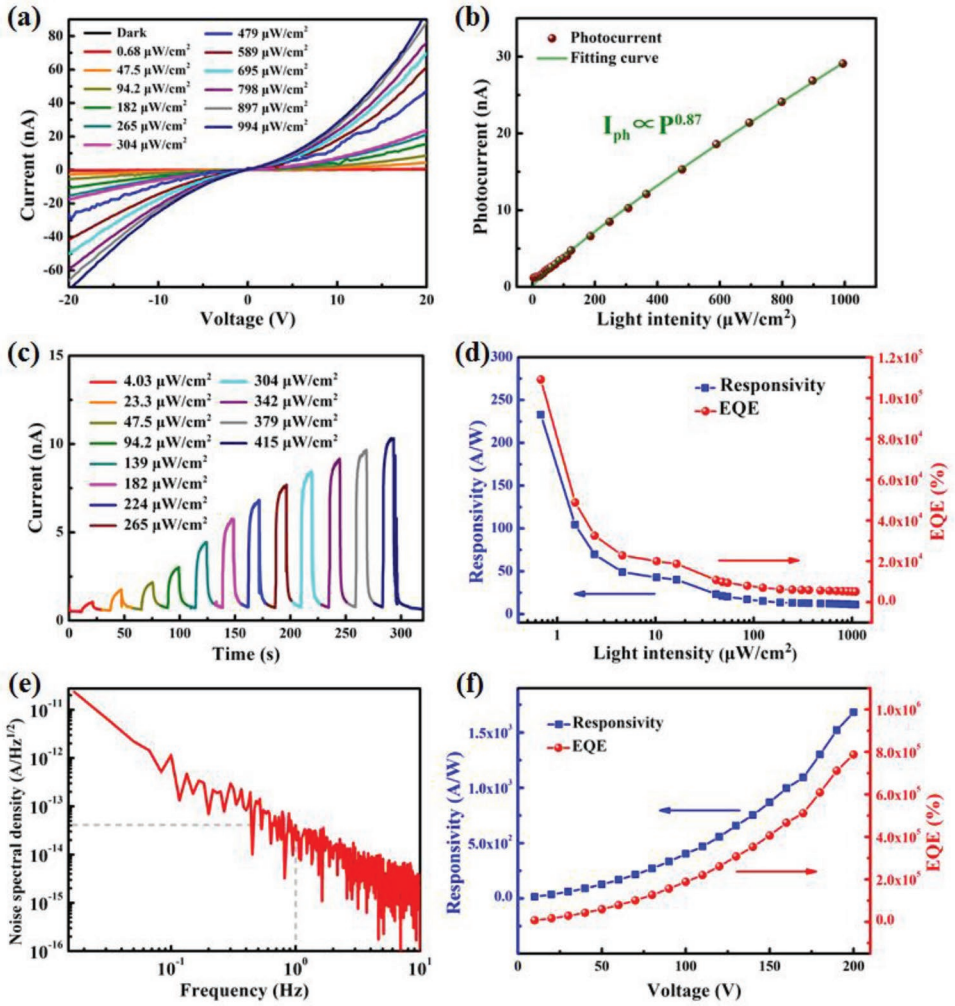

Figure 4. a) *I–V* curves and c) time-dependent photoresponse of the DUV photodetector under 265 nm illumination with varied light intensities. b) The photocurrent at 10 V bias as a function of light intensity. d) Dependence of responsivity and EQE on the light intensity. e) Analysis of noise spectral density of the device. f) Dependence of responsivity and EQE on the applied bias voltage.

voltages (see **Table 1**).[18,21,26,27,29] In addition, similar to the observations in other photodetectors,[39–41] both R and EQE declined gradually with increasing light intensity (Figure 4c), which again manifests the presence of photocurrent recombination loss in the DUV photodetector. Under light illumination with an elevated intensity, the recombination of photocarriers will be accelerated due to increased concentration of charge carriers in the NWs.[40]

In addition, we also studied the specific detectivity (D^*), a key parameter reflecting the ability of photodetector to detect the weakest light signal. The D^* is usually expressed as[42]

$$D^* = \frac{(S\Delta f)^{1/2}}{\mathrm{NEP}} \tag{2}$$

where Δf and NEP denote bandwidth and noise equivalent power, respectively. The NEP, representing the lowest incident optical power needed to attain a signal-to-noise ratio of 1 at 1 Hz, is defined as[43]

$$\mathrm{NEP} = \frac{\overline{i_n^2}^{1/2}}{R} \tag{3}$$

where $\overline{i_n^2}^{1/2}$ is the root-mean-square value of the noise current. As presented in Figure 4e, the value was deduced to be $\approx 4.04 \times 10^{-14}$ A $\mathrm{Hz}^{-1/2}$ for our β-Ga_2O_3 NWs-based DUV photodetector by performing Fourier transformation of the dark current (Figure S3b, Supporting Information). According to the above equations, the NEP was calculated to be $\approx 1.73 \times 10^{-16}$ W $\mathrm{Hz}^{-1/2}$, which led to a D^* value of $\approx 8.16 \times 10^{12}$ Jones. Such a high D^* value is comparable with the values of a single-crystalline Sn-doped β-Ga_2O_3 wafer/graphene heterojunction DUV photodetector ($\approx 10^{13}$ Jones)[17] and a exfoliated single-crystalline β-Ga_2O_3 microflake MSM DUV photodetector with graphene electrodes ($\approx 1.45 \times 10^{12}$ Jones).[22]

It is observed that such a DUV photoresponse depended strongly on the applied bias voltage as well. Figure S5a (Supporting Information) depicts the *I–V* characteristics of another

Table 1. Comparison of key parameters of the β-Ga_2O_3 NWs-based DUV photodetector with similar devices.

Method	Dark current [A]	I_{light}/I_{dark} ratio	Responsivity [A W^{-1}]	EQE	τ_r/τ_d [s]	Ref.
CVD	$\approx 10^{-13}$	–	$\approx 10^2$ (30 V)	–	11.8/<0.3	[27]
CVD	1×10^{-13}	$\approx 10^5$	850 (20 V)	4.2×10^5%	<0.3/<0.3	[28]
CVD	1×10^{-13}	$\approx 10^3$	547 (6 V)	2.72×10^5%	1/<0.6	[30]
MOCVD[a)]	2.44×10^{-10}	≈ 10	8×10^{-4} (10 V)	–	–	[29]
CVD	1.33×10^{-10}	–	3.72×10^{-4} (5 V)	–	–	[23]
PLD[b)]	1.07×10^{-8}	1.6	–	–	4.3/76.1	[21]
CVD	1.5×10^{-11}	$\approx 10^2$	–	–	0.45/0.09	[25]
CVD	2×10^{-13}	$\approx 10^4$	$\approx 10^{-2}$ (5 V)	–	0.02/10	[26]
CVD	8×10^{-12}	≈ 50	377 (10 V)	2×10^5%	0.21/<0.5	[18]
CVD	7.73×10^{-11}	$\approx 10^3$	233 (10 V)	1×10^5%	0.48/0.04	This work

[a)]Metal–organic chemical vapor deposition; [b)]Pulsed laser deposition.

β-Ga_2O_3 NWs-based DUV photodetector in dark and under 265 nm illumination (86 μW cm^{-2}) at a bias voltage ranging from −200 to 200 V. Clearly, the device was highly sensitive to the DUV irradiation in a wide working bias region. Furthermore, as observed in the time-dependent photoresponse (Figure S5b, Supporting Information), the device can operate properly with good reproducibility and stability even at a very large bias voltage of 200 V. These findings suggest that the present DUV photodetector can potentially be used for application in high-power optoelectronics. The bias voltage–dependent R and EQE were then studied, as depicted in Figure 4f. It was found that both the R and EQE rise gradually with increasing bias voltage, and the maximum values can reach as high as ≈1680 A W^{-1} and $\approx 8.0 \times 10^5$%, respectively, at an applied bias of 200 V. Such a relationship is reasonable because a large electric field can significantly enhance the separation and drift velocity of photocarriers and, therefore, reduce their recombination, which is helpful for photoresponse improvement.

Furthermore, the response speed that reflects the ability of a photodetector to detect rapidly switched optical signal was studied. **Figure 5**a plots the temporal photoresponse of the β-Ga_2O_3 NWs-based DUV photodetector to the pulsed 265 nm light illuminations with varied frequencies of 1, 10, 20, and 50 Hz. Apparently, for all the frequencies, the detector was able to track the switchable illumination with well-identified high- and low-current states. However, due to the relatively long rise time, the photocurrent fails to reach its maximum value at the first cycle of operation, and it exhibited a gradually increase trend with the increment in operating cycle when the frequency exceeds 10 Hz. From a single magnified response curve at 1 Hz (Figure 5b), the rise and decay times (τ_r and τ_d) of the detector were estimated to be 0.48 and 0.04 s, respectively.[44] Note that such a response speed was comparable to or even faster than that of many β-Ga_2O_3 NWs- or NBs-based DUV photodetectors (see Table 1).[21,25–27,30] It is believed that the performance of the β-Ga_2O_3 NWs-based DUV photodetector could be further improved by means of enhancing the quality of the NWs, optimizing the device design such as employing MSM structure with interdigital electrodes or Schottky contacts, constructing Schottky barrier or avalanche photodiodes, and so on.[14,45,46]

The long-term air stability representing a critical parameter for practical application was also explored. The photoresponse properties were re-examined and compared after placing the DUV photodetector at ambient conditions for about 2 months without any protection. As displayed in Figure S6 (Supporting Information), both I–V curve under DUV light illumination and time-dependent photoresponse kept almost invariant after storage, suggesting good ambient stability of our device.

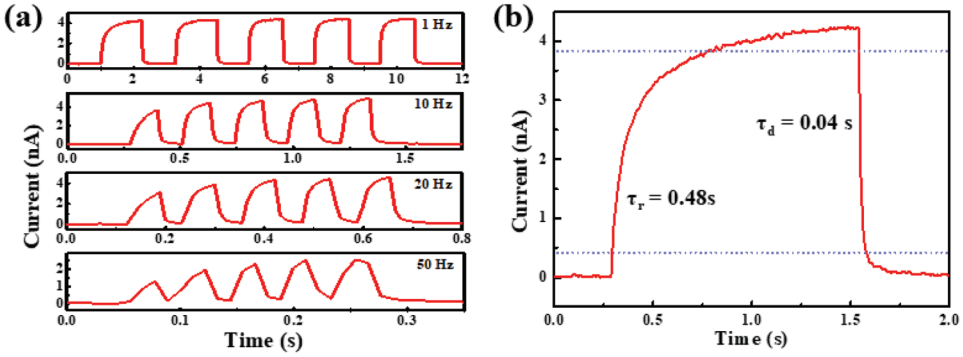

Figure 5. a) Photoresponse curve of the detector to repeatable DUV light with frequencies of 1, 10, 20, and 50 Hz. b) A single magnified curve measured at 1 Hz for determining rise time (τ_r) and decay time (τ_d).

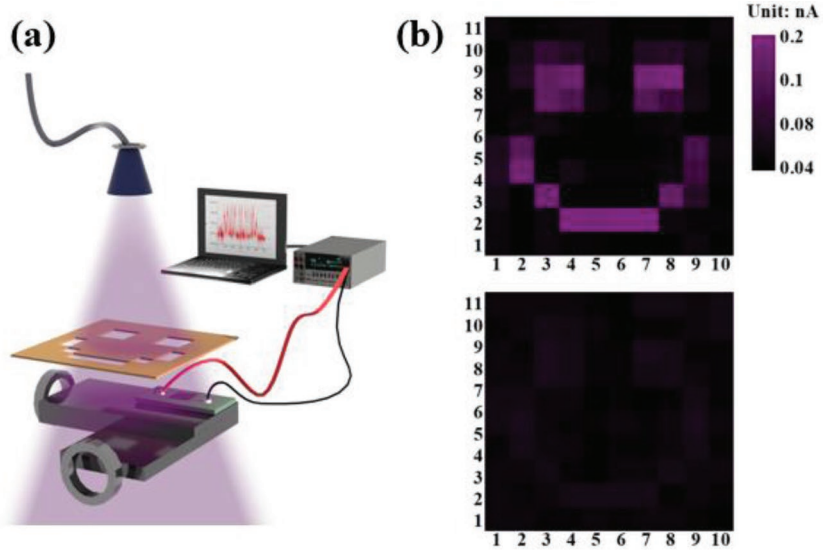

Figure 6. a) Schematic illustration of the DUV imaging system. b) The corresponding 2D current mapping under 265 nm (top panel) and 365 nm (bottom panel) illumination.

Lastly, the possibility of the present photodetector for DUV imaging was explored by employing a setup schematically shown in **Figure 6**a. A laser with a wavelength of 265 or 365 nm was employed to illuminate a lab-built mask with an open "smiley face" pattern (5 cm × 5 cm), while the NWs-based photodetector was fixed to an automatic placement system behind the mask. The system controlled by a computer then driven the detector to progressively scan horizontally (*X*-axis) and vertically (*Y*-axis), and the photocurrent of each pixel was recorded and incorporated into a 2D current mapping system. As displayed in Figure 6b, the shape of the "smiley face" pattern can be clearly distinguished upon 265 nm illumination. However, when the illumination was replaced with 365 nm UV light, no image can be collected by the system. These results suggest that the current imaging system has a relatively high fidelity characteristic for DUV illumination, and the β-Ga_2O_3 NWs-based DUV photodetector holds great possibility for future DUV optoelectronic devices and systems.

3. Conclusion

In summary, we have reported a catalyst-free VS growth technique for synthesizing β-Ga_2O_3 NWs with single-crystalline quality. A photodetector based on such β-Ga_2O_3 NWs exhibited high sensitivity to 265 nm DUV illumination with I_{light}/I_{dark} ratio, responsivity, specific detectivity, and response speed reaching $\approx 10^3$, ≈ 233 A W^{-1}, $\approx 8.16 \times 10^{12}$ Jones, and 0.48/0.04 s, respectively. In addition, the device also displayed a decent DUV/visible (250 nm–405 nm) rejection ratio exceeding 10^2 with an abrupt response cutoff at the wavelength of ≈290 nm. The responsivity can be further enhanced to as high as ≈1680 A W^{-1} by applying a high bias voltage of 200 V, implying the possibility of the current DUV photodetector for high-power optoelectronic applications. Further image-sensing characterization reveals that the β-Ga_2O_3 NWs-based detector was able to record a simple "smiley face" image produced by DUV light with a reasonable spatial resolution. It is expected that the present β-Ga_2O_3 NWs-based DUV photodetector may find potential application in future DUV optoelectronic devices and systems.

4. Experimental Section

Material Preparation and Characterization: The β-Ga_2O_3 NWs used here were grown in a high-temperature tube furnace via a catalyst-free VS mechanism, as schematically shown in Figure S1a (Supporting Information). Liquid metallic Ga was placed on an alumina boat in the central region of a horizontal quartz tube. An alumina substrate, ultrasonically cleaned sequentially with acetone, alcohol, and deionized water, respectively, was placed downstream in the tube. The quartz tube was sealed, and a constant flow of oxygen with a flow rate of 20 or 50 SCCM was introduced through the tube after evacuating. The pressure in the tube was kept at ≈100 Pa. Then the furnace was heated to various growth temperatures of 700, 900, and 1100 °C at an elevating temperature speed of 18 °C min^{-1}, and maintained at this temperature for 60 min. After growth, the tube furnace was cooled down naturally, and the white product of β-Ga_2O_3 NWs was formed on the alumina substrate. The morphology of the as-grown products was observed using a FESEM instrument (Quanta, FEG 250) equipped with an energy-dispersive spectrometer. The crystal structure of the NWs was investigated using a FETEM instrument (JEOL JEM-2100F). The XRD pattern was recorded via an X-ray diffractometer (X'Pert PRO MPD). The absorption spectrum was recorded on a CARY 5000 UV–VIS(NIR) spectrophotometer. The XPS measurement was carried out using a monochromatic Al Kα source produced by the XPS system (Thermo ESCALAB250 X-ray photoelectron spectroscopy).

Device Fabrication and Analysis: Figure S2 (Supporting Information) illustrates the processing steps for constructing the β-Ga_2O_3 NWs-based DUV photodetectors. Briefly, the β-Ga_2O_3 NWs were removed from the growth substrate and dispersed into alcohol with the desired density. Then, the NWs were transferred onto a cleaned SiO_2/Si substrate by carefully dropping the alcohol containing NWs onto the substrate. Afterward, Au electrodes (50 nm) were deposited using a lab-built shadow mask via high-vacuum electron-beam evaporation. DUV photodetectors were formed when β-Ga_2O_3 NWs contacted with Au electrodes at opposite ends. To improve the contact between NWs and Au electrodes, the substrate was then annealed at 500 °C for 1 min under the protection of Ar gas in a rapid thermal annealing furnace (MTI, RTP-1000D4). Characterization of the electrical properties was carried out by using a semiconductor parameter analyzer (Keithley 4200-SCS) on a probe station. For photoresponse study, UV light-emitting diodes (LEDs) with wavelengths of 265 (Thorlabs M265L3) and 365 (Thorlabs M365LP1) were used as light sources. The spectral response was investigated by using a lab-built optoelectronic system including a light source (LE-SP-LS-XE) and monochromator (LE-SP-M300). The intensity of all light sources was carefully calibrated using a power meter (Thorlabs GmbH., PM 100D) prior to measurement. All measurements were carried out in air at room temperature.

Supporting Information

Supporting Information is available from the Wiley Online Library or from the author.

Acknowledgements

This work was supported by the National Natural Science Foundation of China (NSFC, Grant Nos. 61575059, 61675062, and 21501038) and the Fundamental Research Funds for the Central Universities (Grant Nos. JZ2018HGPB0275, JZ2018HGTA0220, and JZ2018HGXC0001).

Conflict of Interest

The authors declare no conflict of interest.

Keywords

β-Ga_2O_3, catalyst-free growth, DUV photodetectors, image sensors, nanowires

Received: July 24, 2019
Revised: September 22, 2019
Published online:

[1] H. Chen, K. Liu, L. Hu, A. A. Al-Ghamdi, X. Fang, *Mater. Today* **2015**, *18*, 493.
[2] L. Sang, M. Liao, M. Sumiya, *Sensors* **2013**, *13*, 10482.
[3] C. Xie, X. T. Lu, X. W. Tong, Z. X. Zhang, F. X. Liang, L. Liang, L. B. Luo, Y. C. Wu, *Adv. Funct. Mater.* **2019**, *29*, 1806006.
[4] E. Monroy, F. Omn s, F. Calle, *Semicond. Sci. Technol.* **2003**, *18*, R33.
[5] Y. J. Lu, C. N. Lin, C. X. Shan, *Adv. Opt. Mater.* **2018**, *6*, 1800359.
[6] J. Y. Tsao, S. Chowdhury, M. A. Hollis, D. Jena, N. M. Johnson, K. A. Jones, R. J. Kaplar, S. Rajan, C. G. Van de Walle, E. Bellotti, C. L. Chua, R. Collazo, M. E. Coltrin, J. A. Cooper, K. R. Evans, S. Graham, T. A. Grotjohn, E. R. Heller, M. Higashiwaki, M. S. Islam, P. W. Juodawlkis, M. A. Khan, A. D. Koehler, J. H. Leach, U. K. Mishra, R. J. Nemanich, R. C. N. Pilawa-Podgurski, J. B. Shealy, Z. Sitar, M. J. Tadjer, A. F. Witulski, M. Wraback, J. A. Simmons, *Adv. Electron. Mater.* **2018**, *4*, 1600501.
[7] D. Walker, V. Kumar, K. Mi, P. Sandvik, P. Kung, X. H. Zhang, M. Razeghi, *Appl. Phys. Lett.* **2000**, *76*, 403.
[8] G. Parish, S. Keller, P. Kozodoy, J. P. Ibbetson, H. Marchand, P. T. Fini, S. B. Fleischer, S. P. DenBaars, U. K. Mishra, E. J. Tarsa, *Appl. Phys. Lett.* **1999**, *75*, 247.
[9] L. K. Wang, Z. G. Ju, J. Y. Zhang, J. Zheng, D. Z. Shen, B. Yao, D. X. Zhao, Z. Z. Zhang, B. H. Li, C. X. Shan, *Appl. Phys. Lett.* **2009**, *95*, 131113.
[10] M. M. Fan, K. W. Liu, X. Chen, X. Wang, Z. Z. Zhang, B. H. Li, D. Z. Shen, *ACS Appl. Mater. Interfaces* **2015**, *7*, 20600.
[11] M. Wei, K. Yao, Y. Liu, C. Yang, X. Zang, L. Lin, *Small* **2017**, *13*, 1701328.
[12] S. J. Pearton, J. Yang, P. H. Cary, F. Ren, J. Kim, M. J. Tadjer, M. A. Mastro, *Appl. Phys. Rev.* **2018**, *5*, 011301.
[13] X. Chen, F. Ren, S. Gu, J. Ye, *Photonics Res.* **2019**, *7*, 381.
[14] B. Zhao, F. Wang, H. Chen, Y. Wang, M. Jiang, X. Fang, D. Zhao, *Nano Lett.* **2015**, *15*, 3988.
[15] G. C. Hu, C. X. Shan, N. Zhang, M. M. Jiang, S. P. Wang, D. Z. Shen, *Opt. Express* **2015**, *23*, 13554.
[16] Z. Wu, G. Bai, Y. Qu, D. Guo, L. Li, P. Li, J. Hao, W. Tang, *Appl. Phys. Lett.* **2016**, *108*, 211903.
[17] W. Y. Kong, G. A. Wu, K. Y. Wang, T. F. Zhang, Y. F. Zou, D. D. Wang, L. B. Luo, *Adv. Mater.* **2016**, *28*, 10725.
[18] J. Du, J. Xing, C. Ge, H. Liu, P. Liu, H. Hao, J. Dong, Z. Zheng, H. Gao, *J. Phys. D: Appl. Phys.* **2016**, *49*, 425105.
[19] W. Feng, X. Wang, J. Zhang, L. Wang, W. Zheng, P. Hu, W. Cao, B. Yang, *J. Mater. Chem. C* **2014**, *2*, 3254.
[20] X. Chen, K. Liu, Z. Zhang, C. Wang, B. Li, H. Zhao, D. Zhao, D. Shen, *ACS Appl. Mater. Interfaces* **2016**, *8*, 4185.
[21] L. H. Zeng, M. Z. Wang, H. Hu, B. Nie, Y. Q. Yu, C. Y. Wu, L. Wang, J. G. Hu, C. Xie, F. X. Liang, L. B. Luo, *ACS Appl. Mater. Interfaces* **2013**, *5*, 9362.
[22] S. Oh, C. K. Kim, J. Kim, *ACS Photonics* **2018**, *5*, 1123.
[23] W. Y. Weng, T. J. Hsueh, S. J. Chang, G. J. Huang, S. C. Hung, *IEEE Trans. Nanotechnol.* **2011**, *10*, 1047.
[24] C. Xie, F. Yan, *Small* **2017**, *13*, 1701822.
[25] P. Feng, J. Y. Zhang, Q. H. Li, T. H. Wang, *Appl. Phys. Lett.* **2006**, *88*, 153107.
[26] Y. Li, T. Tokizono, M. Liao, M. Zhong, Y. Koide, I. Yamada, J.-J. Delaunay, *Adv. Funct. Mater.* **2010**, *20*, 3972.
[27] L. Li, E. Auer, M. Liao, X. Fang, T. Zhai, U. K. Gautam, A. Lugstein, Y. Koide, Y. Bando, D. Golberg, *Nanoscale* **2011**, *3*, 1120.
[28] R. Zou, Z. Zhang, Q. Liu, J. Hu, L. Sang, M. Liao, W. Zhang, *Small* **2014**, *10*, 1848.
[29] W. Y. Weng, T. J. Hsueh, S. J. Chang, G. J. Huang, S. P. Chang, *IEEE Photonics Technol. Lett.* **2010**, *22*, 709.
[30] W. Tian, C. Zhi, T. Zhai, S. Chen, X. Wang, M. Liao, D. Golberg, Y. Bando, *J. Mater. Chem.* **2012**, *22*, 17984.
[31] J. E. Allen, E. R. Hemesath, D. E. Perea, J. L. Lensch-Falk, Z. Y. Li, F. Yin, M. H. Gass, P. Wang, A. L. Bleloch, R. E. Palmer, L. J. Lauhon, *Nat. Nanotechnol.* **2008**, *3*, 168.
[32] D. E. Perea, J. E. Allen, S. J. May, B. W. Wessels, D. N. Seidman, L. J. Lauhon, *Nano Lett.* **2006**, *6*, 181.
[33] V. Schmidt, J. V. Wittemann, S. Senz, U. Gösele, *Adv. Mater.* **2009**, *21*, 2681.
[34] K. Girija, S. Thirumalairajan, V. R. Mastelaro, D. Mangalaraj, *Anal. Methods* **2016**, *8*, 3224.
[35] C. Yang, H. Liang, Z. Zhang, X. Xia, P. Tao, Y. Chen, H. Zhang, R. Shen, Y. Luo, G. Du, *RSC Adv.* **2018**, *8*, 6341.
[36] Z. X. Zhang, L. H. Zeng, X. W. Tong, Y. Gao, C. Xie, Y. H. Tsang, L. B. Luo, Y. C. Wu, *J. Phys. Chem. Lett.* **2018**, *9*, 1185.
[37] L. H. Zeng, S. H. Lin, Z. J. Li, Z. X. Zhang, T. F. Zhang, C. Xie, C. H. Mak, Y. Chai, S. P. Lau, L. B. Luo, Y. H. Tsang, *Adv. Funct. Mater.* **2018**, *28*, 1705970.
[38] J. Li, L. Niu, Z. Zheng, F. Yan, *Adv. Mater.* **2014**, *26*, 5239.
[39] L. Wang, J. S. Jie, Z. B. Shao, Q. Zhang, X. J. Zhang, Y. Wang, Z. Sun, S. T. Lee, *Adv. Funct. Mater.* **2015**, *25*, 2910.
[40] D. Kufer, I. Nikitskiy, T. Lasanta, G. Navickaite, F. H. L. Koppens, G. Konstantatos, *Adv. Mater.* **2015**, *27*, 176.
[41] Z. Sun, Z. Liu, J. Li, G. Tai, S. P. Lau, F. Yan, *Adv. Mater.* **2012**, *24*, 5878.
[42] F. H. L. Koppens, T. Mueller, P. Avouris, A. C. Ferrari, M. S. Vitiello, M. Polini, *Nat. Nanotechnol.* **2014**, *9*, 780.
[43] C. Xie, C. Mak, X. Tao, F. Yan, *Adv. Funct. Mater.* **2017**, *27*, 1603886.
[44] B. Zhao, F. Wang, H. Chen, L. Zheng, L. Su, D. Zhao, X. S. Fang, *Adv. Funct. Mater.* **2017**, *27*, 1700264.
[45] E. Swinnich, M. N. Hasan, K. Zeng, Y. Dove, U. Singisetti, B. Mazumder, J.-H. Seo, *Adv. Electron. Mater.* **2019**, *5*, 1800714.
[46] J. Bae, H. W. Kim, I. H. Kang, J. Kim, *RSC Adv.* **2019**, *9*, 9678.